The influence of Ti ultrathin insertion layer on the effective magnetic damping and effective spin Hall angle FREE

Zhan Xu ✉ iD ; Grayson Dao Hwee Wong iD ; Jiaxuan Tang; Er Liu iD ; Birte Coester iD ; Feng Xu ✉ iD ; Leixiang Bian; Wen Siang Lew ✉ iD

Check for updates

CrossMark

View Online

Export Citation

The influence of Ti ultrathin insertion layer on the effective magnetic damping and effective spin Hall angle

Zhan Xu,[1,2,3,a)] (iD) Grayson Dao Hwee Wong,[2] (iD) Jiaxuan Tang,[3] Er Liu,[3] (iD) Birte Coester,[2] (iD) Feng Xu,[3,a)] (iD)
Leixiang Bian,[1] and Wen Siang Lew[2,a)] (iD)

AFFILIATIONS

[1]School of Mechanical Engineering, Nanjing University of Science and Technology, Nanjing 210094, China
[2]School of Physical and Mathematical Sciences, Nanyang Technological University, 21 Nanyang Link, Singapore 637371
[3]MIIT Key Laboratory of Advanced Metallic and Intermetallic Materials Technology, School of Materials Science and Engineering,
  Nanjing University of Science and Technology, Nanjing 210094, China

[a)]Authors to whom correspondence should be addressed: zhanxu@njust.edu.cn, xufeng@njust.edu.cn and wensiang@ntu.edu.sg

ABSTRACT

We report the influence of ultrathin Ti insertion layer on the effective magnetic damping and effective spin Hall angle in Co/[Pt/Ti]$_n$/Pt structures via spin-torque ferromagnetic resonance measurements. The effective magnetic damping shows a non-monotonic variation as a function of insertion layers number n, reaching a minimum at $n = 5$. Our analysis shows that when n is less than 5, the damping is mainly related to the thickness of the bottom Pt layer, and when it is greater than 5, the attenuation of the spin currents leads to increased damping. The effective magnetic damping first decreases as the number of layers n increases, reaching a minimum at $n=5$, and then increases with further increases in n. The observation can be ascribed to a competition between the increased longitudinal resistivity, which is due to the strong interfacial scattering, and the reduced effective spin Hall conductivity that originates from the shortening of the carrier lifetime. Additionally, the extracted interfacial spin transparency is found to be improved with the effect of the insertion layer.

Published under an exclusive license by AIP Publishing. https://doi.org/10.1063/5.0146095

The study of the spin–orbit torque (SOT) phenomenon and the engineering of SOT devices have received considerable attention due to their potential application in current-induced magnetization switching, specifically, in high-speed operations and energy-efficient memory devices.[1–5] The SOT phenomenon has been observed in heavy metal/ferromagnetic (HM/FM) bilayer structures, which arises from the interfacial Rashba–Edelstein effect and/or the bulk spin Hall effect (SHE).[6–9] The SHE generates a transverse spin current in the HM layer and diffuses into the FM layer, resulting in a transfer of spin torque to the magnetic moment.[10,11] Effective spin Hall angle (ESHA, θ_{SH}^{eff}) gives the charge current to spin current conversion efficiency, which has been commonly used to quantify the effect due to SOT. A larger ESHA leads to lower energy consumption in devices with SOT-induced magnetization switching. The search for new materials with large ESHA continues, and there are a number of interesting materials reported, for instance, heavy metals,[12–14] alloys,[15–19] antiferromagnet materials,[20–22] topological insulators,[23,24] and transition metal dichalcogenides (TMDs).[25,26]

Using interface engineering efforts to enhance the SOT has attracted strong interest, e.g., the insertion of ultrathin films in the HM/FM interface.[27] Nguyen *et al.* reported a considerable SOT enhancement by inserting a thin Hf layer between the Pt and CoFeB layer.[27] Lee *et al.* demonstrated that the SOT in Pt/CoFeB systems is significantly enhanced via a Ti spacer.[28] Other materials, such as, W, Mo, C, and Au, were also found to have a significant influence on SOT efficiency for interface modification.[29–32] In a more recent reference, Zhu *et al.* reported enhanced SOT when ultrathin Ti and Hf layers were inserted into Pt layers.[33,34] However, to minimize the critical switching current in a SOT device, it is essential to achieve a low effective damping factor (α_{eff}) and high θ_{SH}^{eff} simultaneously.[35,36]

In this work, we utilize the spin-torque ferromagnetic resonance (ST-FMR) measurement technique[16–18,37] to investigate the influence of the ultrathin insertion layers on effective magnetic damping, effective spin Hall angle, and interfacial spin transparency. Our measurements reveal that the Ti insertion layer reduces the effective magnetic damping by nearly a factor of two and, concurrently, leads to a two

times higher θ_{SH}^{eff} than the value in Co/Pt. After insertion of the Ti layers, the α_{eff} is found to be strongly dependent on the thickness of the bottom Pt layer. The α_{eff} first decreases as the number of layers n increases, reaching a minimum at $n = 5$, and then increases with further increases in n. The θ_{SH}^{eff} shows the opposite trend due to a competition between the strong interfacial scattering and the reduced carrier lifetime. Furthermore, our measurement reveals that interfacial spin transparency can be improved via Ti insertion layers.

Thin film stacks were deposited on thermally oxidized silicon substrates by DC magnetron sputtering at room temperature. The film stack, as schematically shown in Fig. 1(a), consists of Si(SiO$_2$)/Ti (2 nm)/Co (5 nm)/[Pt (d)/Ti (0.2 nm)]$_n$/Pt (d), where $(n + 1)$ $d = 5$ nm and $n = 0, 1, 3, 4, 5,$ and 7. The base pressure in the sputter chamber was better than 1×10^{-7} mTorr, and the sputtering pressure was set at 3 mTorr. The saturation magnetization, M_S, and the interfacial anisotropy constant, K_S, were measured by using a vibrating sample magnetometer (VSM). The film stacks were patterned into rectangular-shaped strips of 50×10 μm^3 using a combination of electron beam lithography and Ar ion milling techniques. For ST-FMR measurement, Ta (5)/Cu (200)/Pt (3 nm) electrodes were added to the patterned structures by using electron beam lithography and liftoff techniques.

Figures 1(b) and 1(c) show the schematic of the setup with an optical image of the patterned structure for the ST-FMR measurement. A high aspect ratio strip and symmetric three-terminal contact configuration is used to reduce the asymmetric current spreading effect.[38] A radio frequency (RF) current, $I_{c,rf}$, was applied to the microstrip along the longitudinal direction, while an external magnetic field (H) in the sample plane was swept at 45° from 0 to 5000 Oe, with the microwave frequency fixed during each sweep. The $I_{c,rf}$ generates a microwave-frequency SOT on the FM layer. The SOT-induced magnetization precession leads to an anisotropic magnetoresistance effect in the FM layer.[12] The oscillatory resistance, together with RF current, gives rise to a rectified mixing voltage V_{mix}, which was measured by using a bias tee. For the ST-FMR measurement, the input microwave power was varied from 10 to 20 dBm, and the measured DC voltage was in the
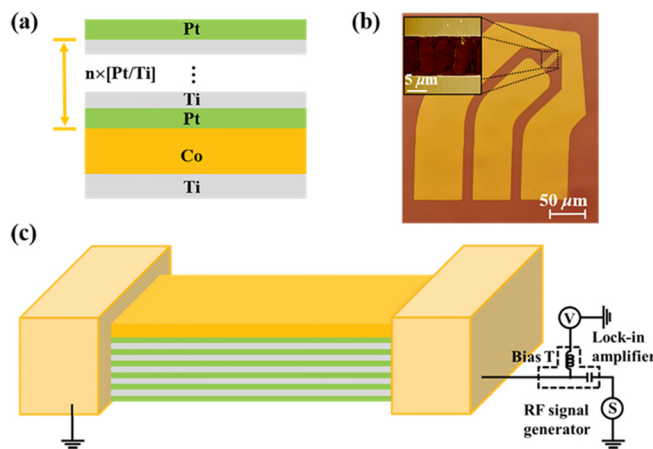
linear regime with increasing power. The measured θ_{SH}^{eff} was independent of the applied RF power, indicating that the microwave heating effect is relatively negligible (see Fig. S1 in the supplementary material for details). All measurements were performed at the RF power of 18 dBm. The ST-FMR spectra were measured for microwave frequencies from 8 to 23 GHz for all samples. All measurements were conducted at room temperature.

Figure 2(a) illustrates a weak increase in saturation magnetization (M_s) with increasing n. The measured M_s for $n = 0$ is 1067.8 emu/cc, smaller than 1440 emu/cc for the bulk Co. The surface anisotropy constant (K_s) was determined using the relation $H_k \approx 4\pi M_s - 2K_s/M_s t$, where H_k was the anisotropy field determined from the intersection point of the M–H loops along the out-of-plane and in-plane directions characterized by the VSM, t is the Co layer thickness.[39,40] The measured K_s decreases non-monotonically with larger n values, and the minimal K_s value, i.e., 0.47 erg/cm^2, was obtained at $n = 5$, as shown in Fig. 2(a). For the case $n = 0$, the measured K_s is 1.02 erg/cm^2, which is close to the value reported by Pai et $al.$[40] in their Co/Pt structure, i.e., 1.10 ± 0.13 erg/cm^2. The longitudinal resistivity ρ_{xx} for each Pt/Ti multilayer sample was determined by measuring the resistance enhancement of the stack with n insertions relative to the reference stack with $n = 0$. The measured ρ_{xx} for Pt/Ti multilayer as a function of n is shown in Fig. 2(b). By increasing n from 0 to 7, ρ_{xx} increases monotonically from 25.3 $\mu\Omega$ cm for $n = 0$–92.5 $\mu\Omega$·cm for $n = 7$ owing to the enhanced interfacial scattering. According to previous reports,[33,34] it is reasonable to assume that the Elliot–Yafet spin relaxation mechanism plays a dominant role here,[41,42] in which the spin diffusion length λ_{sd} is approximately inversely proportional to ρ_{xx}. The obtained λ_{sd} values decrease from 2.8 to 0.71 nm as n increases from 0 to 7, as shown in Fig. 2(b). It is interesting to note that d is more significant than λ_{sd} from $n = 0$ to $n = 4$, and when $n = 5$, λ_{sd} is very close to d ($d = 0.84$ nm). By further increasing n to 7, d becomes smaller than λ_{sd}.

Figure 3(a) shows the ST-FMR spectra signal V_{mix} for Pt/Ti devices with $n = 5$ measured at a frequency range of 8–16 GHz. Figure 3(b) shows the curve fitting of an ST-FMR spectrum measured at 12 GHz. The signals have superimposed symmetric and antisymmetric Lorentzian components, which are presented in Fig. 3(b) as the red and blue curves, respectively. The measured mixing DC voltage V_{mix} is expressed as[12,20]

$$V_{mix} = S\frac{(\Delta H)^2}{(\Delta H)^2 + (H - H_{res})^2} + A\frac{\Delta H(H - H_{res})}{(\Delta H)^2 + (H - H_{res})^2} + V_0,$$

(1)

where ΔH, H_{res}, V_0, S, and A are the resonance linewidth, the resonance magnetic field, the offset voltage, and the amplitudes of the symmetric and anti-symmetric components of the mixing voltage, respectively. In the ST-FMR signal, the symmetric component is proportional to the damping-like effective torque, and the anti-symmetric component is due to the sum of the Oersted field torque and the field-like effective torque.[12,13,20] The effective magnetization $4\pi M_{eff}$ values have been extracted by fitting the resonance frequency f as a function H_{res} in Fig. 3(c). Since the in-plane magnetic anisotropy is negligibly small, the Kittel equation can be written as $f = (\gamma/2\pi)[H_{res} (H_{res} + 4\pi M_{eff})]^{1/2}$, where γ is the gyromagnetic ratio.[43] The obtained $4\pi M_{eff}$ for $n = 5$ is 1.329 T, which is consistent with the M_s value
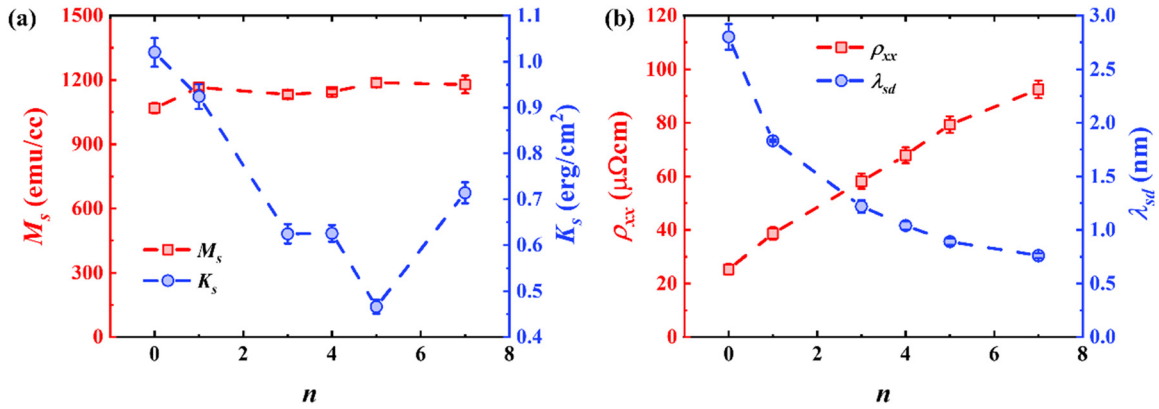

FIG. 1. Schematic illustration of the sample structure (**a**) and the measurement setup (**c**). Optical image of the fabricated device and electrodes (**b**). Inset is the AFM image of the micro-strip.

FIG. 2. M_s, K_s(a), ρ_{xx}, and λ_{sd} (b) as a function of n.

extracted from the VSM results considering the out-of-plane anisotropy field contribution to the effective magnetization. Furthermore, K_s can be obtained from the relationship of $4\pi M_{eff}$. For thin films, the bulk anisotropy related to in-plane crystalline anisotropy and shape anisotropy is negligible compared to the interfacial anisotropy, the effective magnetization can be expressed as $4\pi M_{eff} = 4\pi M_s - 2K_s/$

$M_s t$.[44] The obtained K_s are in good agreement with the VSM measurement (see Fig. S2, K_s from ST-FMR in the supplementary material for details).

With a linear fit obtained using the equation $\Delta H = \Delta H_{inh} + 2\pi f \alpha_{eff}/\gamma$,[45] the α_{eff} and the inhomogeneity linewidth broadening (ΔH_{inh}) of the $n = 5$ are determined from the Fig. 3(d). From the
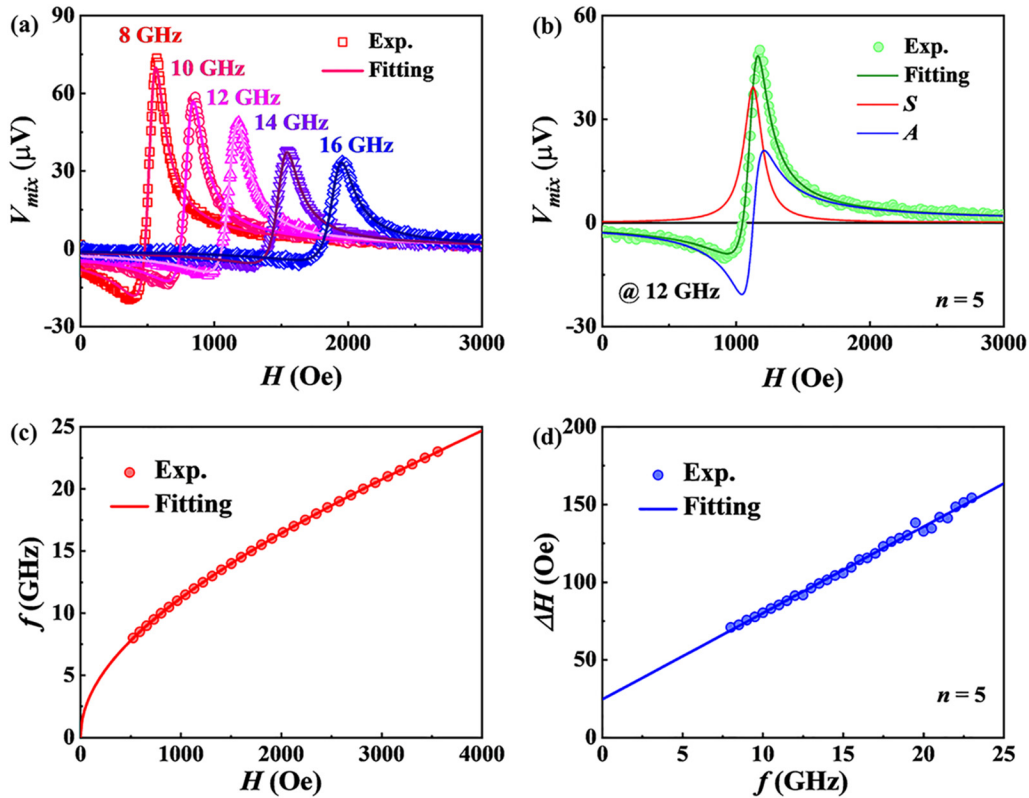

FIG. 3. ST-FMR measurements for the $n = 5$ devices. (a) The ST-FMR spectra from 8 to 16 GHz. (b) V_{mix} along with the fitted (green), symmetric (S, red), and asymmetric (A, blue) Lorentzian functions used for the fitting measured at 12 GHz. (c) The measured f as a function of H_{res}. (d) The ΔH as a function of f.

fitting, the value of α_{eff} is found to be 0.0079, which is lower than the previously reported value of Co/Pt,[40] indicating that the insertion layer can suppress the α_{eff}. The extracted ΔH_{inh} is found to be 24.5 Oe, indicating a flat interface between the Pt/Ti multilayer and Co layer.[12,46] Moreover, the ΔH vs f response as plotted in Fig. 3(d) shows no deviation from rigorous linear relation over the entire frequency range, indicating a negligible contribution from the two-magnon scattering mechanisms in the film that would result in a non-linear trend.[35,47,48]

The dependence of the α_{eff} on n is given in Fig. 4(a). As n increases from 0 to 7, α_{eff} dropped from 0.0130 at $n = 0$ ($d = 5$ nm) to a minimal value of 0.0079 at $n = 5$ ($d = 0.84$ nm) and then quickly increased to 0.0124 at $n = 7$ ($d = 0.625$ nm). However, as compared to the intrinsic damping factor of the Co thin film (0.004–0.006),[49] the effective damping is still enhanced in the [Pt/Ti]$_n$/Pt/Co multilayer. Thus, it is essential to analyze the mechanism of the additional damping. Since the atomic spin–orbit coupling of Ti is quite small and away from the Co layer,[34] the additional damping due to the Ti insertion layers induced by the spin pumping can be excluded. Second, for the present Pt/Ti multilayer, the influence of the magnetic proximity effect on the effective magnetic damping can be excluded owing to the magnetic moments of Pt atoms being negligible here.[50,51]

The additional damping should be due to the angular momentum induced by the spin pumping.[35,52] For non-magnetic metals, the spin pumping-induced damping enhancement is mostly related to bulk spin absorption. However, due to the suppression of spin current into the bulk by the Ti insertion layer,[33] the bottom Pt layer may predominantly contribute to the additional damping. To confirm this mechanism, the α_{eff} as a function of the thickness of bottom Pt layer was plotted and fitted with the spin pumping model, which can be expressed as[53]

$$\alpha_{eff} = \alpha_{FM} + \frac{g\mu_B}{4\pi M_s t} G^{\uparrow\downarrow}\left(1 - e^{\frac{-2d}{\lambda_{sd}}}\right), \tag{2}$$

where g is the spectroscopic splitting factor, μ_B is the Bohr magneton, α_{FM} is the intrinsic damping of the FM layer, and $G^{\uparrow\downarrow}$ is the spin mixing conductance. Using different λ_{sd} obtained from Fig. 2(b), the thickness of the Pt layer dependence of α_{eff} is fitted in Fig. 4(b). For all $d \geq \lambda_{sd}$ samples (n from 0 to 5) fit well with $\lambda_{sd} = 2.8$ nm, indicating the bottom Pt layer may play a dominant role in the increased damping. From the fitting, the obtained $G^{\uparrow\downarrow}$ is found to be 31.5 nm^{-2}, which is consistent with the previous reports.[40,46] This spin mixing conductance also indicates the absence of significant intermixing of Pt
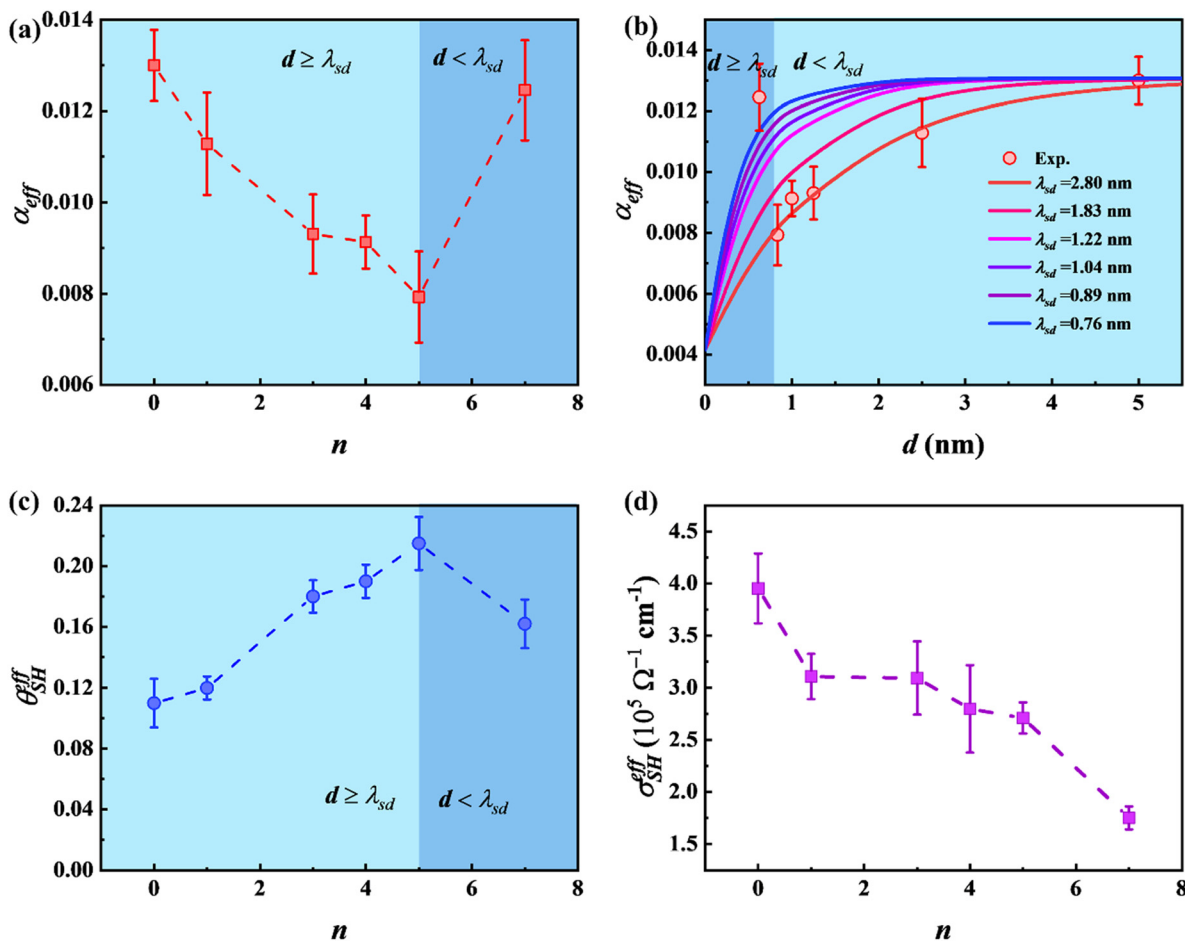

FIG. 4. The n (a) and thickness of each Pt layer (b) dependence of α_{eff}. The θ_{SH}^{eff} (c) and σ_{SH}^{eff} (d) as a function of n.

impurities within the magnetic layer near the Co/Pt interface. Furthermore, for $n = 7$ where $d < \lambda_{sd}$, the strong attenuation of the spin currents that diffuse from the bottom Pt layer to the FM interface leads to the abrupt increase in damping.[34] Additionally, this behavior for the enhanced damping as a function of d is inconsistent with the magnetic proximity effect-induced additional damping, which is a quasilinear thickness dependence of damping, indicating that there is no evidence of the magnetic proximity effect having an effect on the α_{eff}.[49]

From the line shape of the ST-FMR spectra, the θ_{SH}^{eff}, which is the ratio of the spin current density to the RF current density, can be extracted for a qualitative dependence according to the ST-FMR theory.[12,20] The θ_{SH}^{eff} is given by[13]

$$\theta_{SH}^{eff} = \frac{eJ_S}{J_C} = \frac{S}{A} \frac{e\mu_0 M_S td}{\hbar}\left(1 + \frac{4\pi M_{eff}}{H_{res}}\right)^{\frac{1}{2}}, \quad (3)$$

where J_S is the spin current density generated within the heavy metal, and J_C is the applied charge current density. The θ_{SH}^{eff} increases non-monotonically with n increasing, with the maximal values at $n = 5$, as shown in Fig. 4(c). The value of $n = 0$ is consistent with a previous report by comparison. A significant ($\sim$110%) enhancement of θ_{SH}^{eff} is found from 0.10 for $n = 0$ to 0.21 for $n = 5$. Since Ti does not contribute to the generation of the spin current due to its negligible bulk spin–orbit coupling.[33] The insertion layer has caused an increase in resistivity, which raises the scattering rate. It demonstrates that the θ_{SH}^{eff} is enhanced by the Ti insertion layer. To understand the non-monotonically behavior of θ_{SH}^{eff}, the effective spin Hall conductivity σ_{SH}^{eff} is determined from the relation $\sigma_{SH}^{eff} = \theta_{SH}^{eff}/\rho_{xx}$, as shown in Fig. 4(d). With the n increasing from 0 to 7, the σ_{SH}^{eff} decreases rapidly due to the decrease in carrier lifetime according to a previous report.[54] Tanaka et al. calculated that when the ρ_{xx} is larger than 30 $\mu\Omega$ cm, the Pt thin film is in the dirty-metal regime, where the shortening of the carrier lifetime should lead to a sharp decrease in the intrinsic spin Hall conductivity regardless of the crystalline order.[55] Therefore, the non-monotonically behavior of θ_{SH}^{eff} can be attributed to a competition between increased ρ_{xx} and decreased σ_{SH}^{eff}.[33,34] When $n \leq 5$, the interfacial scattering is the dominant mechanism. As the number of insertion layers increases, an enhanced θ_{SH}^{eff} is observed. When n is greater

than 5, at this point, the decrease in carrier lifetime due to insertion layers is greater than the increase in the interfacial scattering contribution, so the θ_{SH}^{eff} decreases with the continued increase in n.

To understand the contributions of the spin current attenuation, a [Pt 0.84/Cu 0.2 nm]5/Pt 0.84/Co 5 nm multilayer structure was fabricated. Cu has a very weak spin–orbit interaction and a very long spin diffusion length.[56] The spin current undergoes weak dissipation in the ultrathin Cu spacer but flows into and dissipates in the Pt films. Thus, an ultrathin Cu insertion layer is not expected to affect the spin pumping effect but can change other interface effects. However, we obtained a reduced α_{eff} (0.0083) and an enhanced θ_{SH}^{eff} (0.16) in the Pt/Cu multilayer compared to that in Co/Pt bilayer (Fig. S4, Pt–Cu multilayer in the supplementary material), suggesting that the attenuation of spin current is due to the interface. The θ_{SH}^{eff} in Pt/Cu multilayer is smaller than that in Pt/Ti multilayer because the Cu induced interfacial scattering is smaller than the Ti insertion layer induced. It is noted that the θ_{SH}^{eff} of Pt/Cu multilayer is larger than in the $Cu_{1-x}Pt_x$ alloy, indicating using the insertion layer is a more efficient way to engineer the θ_{SH}^{eff}.

Furthermore, the interfacial spin transparency is determined to better understand the role of the insertion layer. Two major contributions are essential to T: (1) interfacial spin memory loss (SML) owing to spin-flip scattering at the interface[39,57–59] and (2) spin backflow (SBF) depends on spin mixing conductance of the interface.[60,61] Zhu et al. reported that the SML is linear to the interfacial perpendicular magnetic anisotropy energy density (K_s) of the HM/FM interface,[39] for the in-plane magnetized Co/Pt interface, there are $T_{SML} \approx 1 - 0.23 K_s$ with K_s in erg/cm^2. Using the obtained K_s from VSM, the T_{SML} is varied from 0.76 to 0.89, as shown in Fig. 5(a), suggesting, at the maximum, a 24% attenuation at the interface due to the SML. On the other hand, according to the drift-diffusion model, the efficiency of spin transport through the interface depends on the SBF, which can be estimated from[46,56]

$$T_{SBF} = \frac{G_{eff}^{\uparrow\downarrow}\tanh\left(\frac{d}{2\lambda_{sd}}\right)}{G_{eff}^{\uparrow\downarrow}\coth\left(\frac{d}{\lambda_{sd}}\right) + h/2\lambda_{sd}\rho e^2}, \quad (4)$$
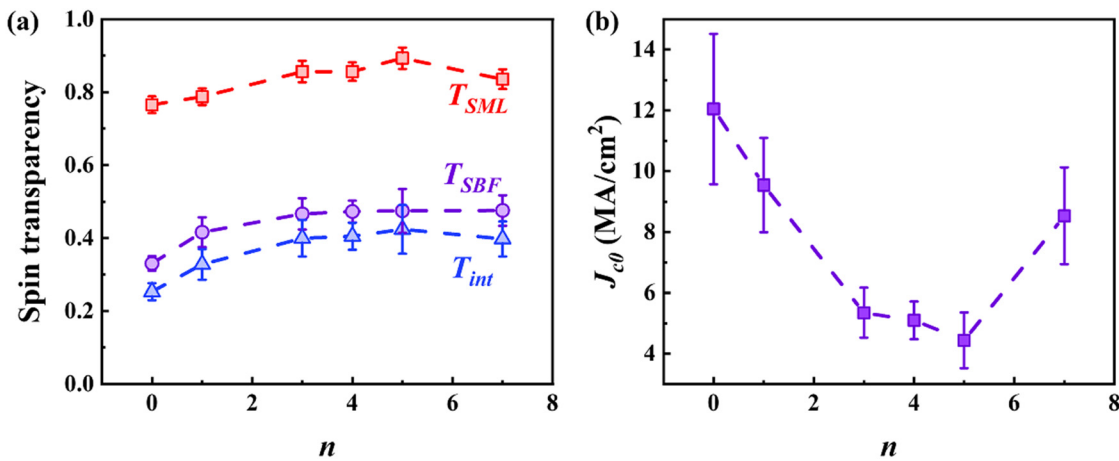

FIG. 5. The obtained spin transparency (a) and the calculated J_{c0} (b) as a function of n.

where $G_{eff}^{\uparrow\downarrow} = G^{\uparrow\downarrow}\left(1 - e^{\frac{-2d}{\lambda_{sd}}}\right)$ is the effective spin mixing conductance, which considers the backflow of spin angular momentum. Figure 5(a) shows the calculated values of the T_{SBF} as a function of n. Due to the rapid decrease in λ_{sd}, T_{SBF} tends to be saturated ($\sim$0.47) for $n \geq 3$, which suggests that the SBF is suppressed due to the Ti insertion layer. Considering both contributions of SML and SBF, $T_{int} \approx T_{SML}T_{SBF}$, the T_{int} is enhanced from 0.25 for $n = 0$ to 0.42 for $n = 5$. In addition, the SBF and SML effect can also affect the magnetic damping. The SML effect at the Pt/FM interfaces as an additional spin sink enhances the effective magnetic damping, while a stronger SBF reduces the spin pumping damping. Based on the above discussion, because of the suppression of the SBF, it should not cause any reductions in damping. The increase in the interfacial spin transparency of the SML due to the insertion layers reduces the scattering of the spin current at the interface, resulting in the reduction of the additional magnetic damping. It can be proved that the interfacial spin transparency can be effectively improved by the insertion layer, which is of great significance for low energy consumption applications of spin current in multilayered devices.[44,56]

Finally, for SOT-MRAM device applications, it is helpful for device reliability to have reduced writing current density to meet high energy efficiency and improved endurance and retention properties.[62] The critical current density for in-plane magnetization switching driven by an in-plane damping-like SOT is given by[35,36]

$$J_{c0} = \frac{2e}{\hbar}\frac{\alpha}{\theta_{SH}}\left(\frac{4\pi M_{eff}}{2}\right)M_S t. \tag{5}$$

Using Eq. (5), the critical switching current density J_{c0} is calculated using the data in Figs. 4(a) and 4(c), and the result is plotted in Fig. 5(b). With increasing n, the J_{c0} exhibits a minimum of 4.4 MA/cm^2 at $n = 5$, approximately 63% less than that in pure Pt due to a combination of lower α_{eff} and larger θ_{SH}, which shows great potential applications as spin Hall material for SOT-MRAM.[36,62]

In conclusion, we have shown the influence of the ultrathin insertion layers on the α_{eff} and θ_{SH}^{eff} in Co/[Pt/Ti]$_n$/Pt multilayers. The α_{eff} decreases with increasing n, while the thickness of the bottom Pt layer d is larger than λ_{sd}. The α_{eff} is found to be strongly dependent on the thickness of the bottom Pt layer after insertion of the Ti layers. By further increasing n, when d is smaller than λ_{sd}, the attenuation of the spin currents leads to an abrupt increase in magnetic damping. The non-monotonic behavior of θ_{SH}^{eff} can be attributed to a competition between ρ_{xx} and the σ_{SH}^{eff}. Moreover, the interfacial spin transparency is enhanced by the insertion layer. Our findings provide an additional avenue for the development of low-energy consumption spintronic devices.

See the supplementary material for the detailed six parts, including input RF power dependence, K_s from ST-FMR, inhomogeneous linewidth broadening, Pt-Cu multilayer, XRD pattern, and frequency dependence of θ_{SH}.

AUTHOR DECLARATIONS
Conflict of Interest

The authors have no conflicts to disclose.

Author Contributions

Zhan Xu: Data curation (equal); Formal analysis (equal); Methodology (equal); Writing – original draft (equal); Writing – review & editing (equal). **Grayson Dao Hwee Wong:** Formal analysis (equal); Methodology (equal). **Jiaxuan Tang:** Investigation (supporting). **Er Liu:** Investigation (supporting); Supervision (supporting). **Birte Coester:** Data curation (supporting). **Feng Xu:** Supervision (equal). **Leixiang Bian:** Writing – review & editing (equal). **Wen Siang Lew:** Supervision (equal); Writing – review & editing (equal).

DATA AVAILABILITY

The data that support the findings of this study are available from the corresponding authors upon reasonable request.

REFERENCES

[1]S. Emori, U. Bauer, S. M. Ahn, E. Martinez, and G. S. D. Beach, Nat. Mater. **12**, 611 (2013).

[2]C. O. Avci, A. Quindeau, C.-F. Pai, M. Mann, L. Caretta, A. S. Tang, M. C. Onbasli, C. A. Ross, and G. S. D. Beach, Nat. Mater. **16**, 309 (2017).

[3]I. M. Miron, T. Moore, H. Szambolics, L. D. Buda-Prejbeanu, S. Auffret, B. Rodmacq, S. Pizzini, J. Vogel, M. Bonfim, A. Schuhl, and G. Gaudin, Nat. Mater. **10**, 419 (2011).

[4]J. Ryu, S. Lee, K. Lee, and B. Park, Adv. Mater. **32**, 1907148 (2020).

[5]Y. Li, K. W. Edmonds, X. Liu, H. Zheng, and K. Wang, Adv. Quantum Technol. **2**, 1800052 (2019).

[6]L. Liu, O. J. Lee, T. J. Gudmundsen, D. C. Ralph, and R. A. Buhrman, Phys. Rev. Lett. **109**, 096602 (2012).

[7]G. Yu, P. Upadhyaya, Y. Fan, J. G. Alzate, W. Jiang, K. L. Wong, S. Takei, S. A. Bender, L. T. Chang, Y. Jiang, M. Lang, J. Tang, Y. Wang, Y. Tserkovnyak, P. K. Amiri, and K. L. Wang, Nat. Nanotechnol. **9**, 548 (2014).

[8]F. Luo, Q. Y. Wong, S. Li, F. Tan, G. J. Lim, X. Wang, and W. S. Lew, Sci. Rep. **9**, 10776 (2019).

[9]W. J. Kong, C. H. Wan, B. S. Tao, C. Fang, L. Huang, C. Y. Guo, M. Irfan, and X. F. Han, Appl. Phys. Lett. **113**, 162402 (2018).

[10]J. Sinova, S. O. Valenzuela, J. Wunderlich, C. H. Back, and T. Jungwirth, Rev. Mod. Phys. **87**, 1213 (2015).

[11]A. Soumyanarayanan, N. Reyren, A. Fert, and C. Panagopoulos, Nature **539**, 509 (2016).

[12]L. Liu, T. Moriyama, D. C. Ralph, and R. A. Buhrman, Phys. Rev. Lett. **106**, 036601 (2011).

[13]Y. Wang, P. Deorani, X. Qiu, J. H. Kwon, and H. Yang, Appl. Phys. Lett. **105**, 152412 (2014).

[14]C.-F. Pai, L. Liu, Y. Li, H. W. Tseng, D. C. Ralph, and R. A. Buhrman, Appl. Phys. Lett. **101**, 122404 (2012).

[15]C. Hu and C. Pai, Adv. Quantum Technol. **3**, 2000024 (2020).

[16]G. D. H. Wong, W. C. Law, F. N. Tan, W. L. Gan, C. C. I. Ang, Z. Xu, C. S. Seet, and W. S. Lew, Sci. Rep. **10**, 9631 (2020).

[17]Z. Xu, G. D. Hwee Wong, J. Tang, E. Liu, W. Gan, F. Xu, and W. S. Lew, ACS Appl. Mater. Interfaces **12**, 32898 (2020).

[18]B. Coester, G. D. H. Wong, Z. Xu, J. Tang, W. L. Gan, and W. S. Lew, J. Magn. Magn. Mater. **523**, 167545 (2021).

[19]U. Shashank, R. Medwal, T. Shibata, R. Nongjai, J. V. Vas, M. Duchamp, K. Asokan, R. S. Rawat, H. Asada, S. Gupta, and Y. Fukuma, Adv. Quantum Technol. **4**, 2000112 (2021).

[20]J. Zhou, X. Wang, Y. Liu, J. Yu, H. Fu, L. Liu, S. Chen, J. Deng, W. Lin, X. Shu, H. Y. Yoong, T. Hong, M. Matsuda, P. Yang, S. Adams, B. Yan, X. Han, and J. Chen, Sci. Adv. **5**, eaau6696 (2019).

[21] M. Arana, M. Gamino, E. F. Silva, V. M. T. S. Barthem, D. Givord, A. Azevedo, and S. M. Rezende, Phys. Rev. B **94**, 144431 (2018).

[22] M. DC, R. Grassi, J.-Y. Chen, M. Jamali, D. Reifsnyder Hickey, D. Zhang, Z. Zhao, H. Li, P. Quarterman, Y. Lv, M. Li, A. Manchon, K. A. Mkhoyan, T. Low, and J.-P. Wang, Nat. Mater. **17**, 800 (2018).

[23] K. Yasuda, A. Tsukazaki, R. Yoshimi, K. Kondou, K. S. Takahashi, Y. Otani, M. Kawasaki, and Y. Tokura, Phys. Rev. Lett. **119**, 137204 (2017).

[24] N. H. D. Khang, Y. Ueda, and P. N. Hai, Nat. Mater. **17**, 808 (2018).

[25] C. K. Safeer, N. Ontoso, J. Ingla-Aynés, F. Herling, V. T. Pham, A. Kurzmann, K. Ensslin, A. Chuvilin, I. Robredo, M. G. Vergniory, F. de Juan, L. E. Hueso, M. R. Calvo, and F. Casanova, Nano Lett. **19**, 8758 (2019).

[26] H. Xu, J. Wei, H. Zhou, J. Feng, T. Xu, H. Du, C. He, Y. Huang, J. Zhang, Y. Liu, H. Wu, C. Guo, X. Wang, Y. Guang, H. Wei, Y. Peng, W. Jiang, G. Yu, and X. Han, Adv. Mater. **32**, 2000513 (2020).

[27] M.-H. Nguyen, K. X. Nguyen, D. A. Muller, D. C. Ralph, and R. A. Buhrman, Appl. Phys. Lett. **106**, 222402 (2015).

[28] H.-Y. Lee, S. Kim, J.-Y. Park, Y.-W. Oh, S.-Y. Park, W. Ham, Y. Kotani, T. Nakamura, M. Suzuki, T. Ono, K.-J. Lee, and B.-G. Park, APL Mater. **7**, 031110 (2019).

[29] S. K. Li, X. T. Zhao, W. Liu, Y. H. Song, L. Liu, X. G. Zhao, and Z. D. Zhang, Appl. Phys. Lett. **114**, 082402 (2019).

[30] H. Almasi, M. Xu, Y. Xu, T. Newhouse-Illige, and W. G. Wang, Appl. Phys. Lett. **109**, 032401 (2016).

[31] D. Li, B. Cui, T. Wang, J. Yun, X. Guo, K. Wu, Y. Zuo, J. Wang, D. Yang, and L. Xi, Appl. Phys. Lett. **110**, 132407 (2017).

[32] M. Mann and G. S. D. Beach, APL Mater. **5**, 106104 (2017).

[33] L. Zhu and R. A. Buhrman, Phys. Rev. Appl. **12**, 051002 (2019).

[34] L. Zhu, L. Zhu, S. Shi, M. Sui, D. C. Ralph, and R. A. Buhrman, Phys. Rev. Appl. **11**, 061004 (2019).

[35] L. Huang, S. He, Q. J. Yap, and S. T. Lim, Appl. Phys. Lett. **113**, 022402 (2018).

[36] D. Lee, J. Kim, H. Park, K.-J. Lee, B.-K. Ju, H. C. Koo, B.-C. Min, and O. Lee, Phys. Rev. Appl. **10**, 024029 (2018).

[37] Z. Xu, G. D. H. Wong, J. Tang, E. Liu, W. Gan, F. Xu, and W. S. Lew, Appl. Phys. Lett. **118**, 062406 (2021).

[38] Q. Liu and L. Zhu, Appl. Phys. Rev. **9**, 041401 (2022).

[39] L. Zhu, D. C. Ralph, and R. A. Buhrman, Phys. Rev. Lett. **122**, 77201 (2019).

[40] C.-F. Pai, Y. Ou, L. H. Vilela-Leão, D. C. Ralph, and R. A. Buhrman, Phys. Rev. B **92**, 064426 (2015).

[41] R. J. Elliott, Phys. Rev. **96**, 266 (1954).

[42] Y. Yafet, J. Phys. Chem. Solids **21**, 99 (1961).

[43] C. Kittel, Phys. Rev. **73**, 155 (1948).

[44] L. Zhu, D. C. Ralph, and R. A. Buhrman, Phys. Rev. B **99**, 180404 (2019).

[45] E. Liu, T. Fache, D. Cespedes-Berrocal, Z. Zhang, S. Petit-Watelot, S. Mangin, F. Xu, and J. C. Rojas-Sánchez, Phys. Rev. Appl. **12**, 044074 (2019).

[46] W. Zhang, W. Han, X. Jiang, S. H. Yang, and S. S. P. Parkin, Nat. Phys. **11**, 496 (2015).

[47] R. Arias and D. L. Mills, Phys. Rev. B **60**, 7395 (1999).

[48] S. He, Y. Liu, Y. Zheng, Q. Qin, Z. Wen, Q. Wu, Y. Yang, Y. Wang, Y. Feng, K. L. Teo, and C. Panagopoulos, Phys. Rev. Mater. **1**, 064401 (2017).

[49] M. A. W. Schoen, J. Lucassen, H. T. Nembach, B. Koopmans, T. J. Silva, C. H. Back, and J. M. Shaw, Phys. Rev. B **95**, 134411 (2017).

[50] Y. Sun, H. Chang, M. Kabatek, Y.-Y. Song, Z. Wang, M. Jantz, W. Schneider, M. Wu, E. Montoya, B. Kardasz, B. Heinrich, S. G. E. te Velthuis, H. Schultheiss, and A. Hoffmann, Phys. Rev. Lett. **111**, 106601 (2013).

[51] H. Bouloussa, R. Ramaswamy, Y. Roussigné, A. Stashkevich, H. Yang, M. Belmeguenai, and S. M. Chérif, J. Phys. D: Appl. Phys. **52**, 055001 (2019).

[52] Y. Tserkovnyak, A. Brataas, and G. E. W. Bauer, Phys. Rev. Lett. **88**, 117601 (2002).

[53] J. M. Shaw, H. T. Nembach, and T. J. Silva, Phys. Rev. B **85**, 054412 (2012).

[54] L. Zhu, L. Zhu, M. Sui, D. C. Ralph, and R. A. Buhrman, Sci. Adv. **5**, eaav8025 (2019).

[55] T. Tanaka, H. Kontani, M. Naito, T. Naito, D. S. Hirashima, K. Yamada, and J. Inoue, Phys. Rev. B **77**, 165117 (2008).

[56] S. N. Panda, S. Mondal, J. Sinha, S. Choudhury, and A. Barman, Sci. Adv. **5**, eaav7200 (2019).

[57] K. Chen and S. Zhang, Phys. Rev. Lett. **114**, 126602 (2015).

[58] K. Gupta, R. J. H. Wesselink, R. Liu, Z. Yuan, and P. J. Kelly, Phys. Rev. Lett. **124**, 87702 (2020).

[59] K. Dolui and B. K. Nikolić, Phys. Rev. B **96**, 220403 (2017).

[60] P. M. Haney, H.-W. Lee, K.-J. Lee, A. Manchon, and M. D. Stiles, Phys. Rev. B **87**, 174411 (2013).

[61] V. P. Amin and M. D. Stiles, Phys. Rev. B **94**, 104420 (2016).

[62] A. Brataas, A. D. Kent, and H. Ohno, Nat. Mater. **11**, 372 (2012).